Magnetite-Loaded Polymeric Micelles as Ultrasensitive Magnetic-Resonance Probes**

By *Hua Ai*, *Christopher Flask*, *Brent Weinberg*, *Xintao Shuai*, *Marty D. Pagel*, *David Farrell*, *Jeffrey Duerk*, and *Jinming Gao**

Polymeric micelles offer a powerful multifunctional platform for drug delivery and diagnostic imaging applications.[1–5] These nanoconstructs are composed of amphiphilic block copolymers with distinct hydrophobic and hydrophilic segments that can self-assemble into supramolecular core–shell structures (usually 10 to 100 nm) in aqueous solution. The hydrophobic micelle core provides an ideal carrier compartment for hydrophobic agents, and the shell consists of a protective corona that stabilizes the nanoparticles. Many hydrophobic drugs such as paclitaxel and doxorubicin have been successfully loaded inside the micelle core to improve drug solubility and pharmacokinetics.[2,3,6,7] In addition to therapeutic applications, polymeric micelles have also received increasing attention in diagnostic imaging applications. When incorporated into micelles, different types of contrast agents have achieved longer blood half-life, improved biocompatibility, and better contrast.[1]

In this communication, we report the development of superparamagnetic polymeric micelles as a new class of magnetic resonance imaging (MRI) probes with remarkably high spin–spin (T_2) relaxivity and sensitivity. Superparamagnetic iron oxide (SPIO) nanoparticles such as magnetite ($FeO \cdot Fe_2O_3$) are known to have a strong effect on T_2. Better detection sensitivity and slower kidney clearance of SPIO nanoparticles make them advantageous over Gd-based small molecular contrast agents. Currently, most T_2 contrast agents are composed of hydrophilic magnetite nanoparticles dispersed in a dextran matrix.[8,9] In contrast, our micelle design consists of a cluster of hydrophobic magnetite particles encapsulated inside the hydrophobic core of polymeric micelle whose surface is stabilized by a poly(ethylene glycol) (PEG) shell. This unique core–shell composite design has allowed us to achieve an ultrasensitive MRI detection limit of 5.2 $\mu g\,mL^{-1}$ (~5 nM), a sensitivity that promises to expand the "tool box" of MR probes for molecular imaging and image-visible drug-delivery applications.

We used an amphiphilic diblock copolymer of poly(ε-caprolactone)-*b*-poly(ethylene glycol) (PCL-*b*-PEG) for the micelle formation (Fig. 1). This copolymer was synthesized by a ring-opening polymerization of ε-caprolactone using mono-

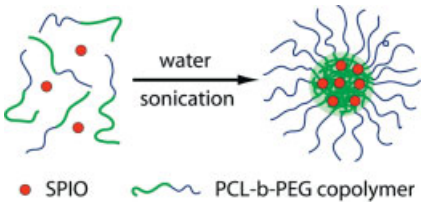

Figure 1. Schematic illustration of SPIO micelle formation.

methoxy-terminated PEG (5 kDa; 1 Da ≃ 1.66×10^{-27} kg) as a macroinitiator and $Sn(Oct)_2$ as a catalyst.[7] The feed ratio was controlled to achieve the final copolymer composition (PCL5k-*b*-PEG5k). The PCL segment has been demonstrated to form crystalline hydrophobic cores, which leads to stable micelle formation with a very low critical micelle concentration.[10] Hydrophobic, single magnetite (Fe_3O_4) nanocrystals were synthesized with precise control of particle diameters (4, 8, and 16 nm) following a published procedure by Sun et al.[11,12] Transmission electron microscopy (TEM) showed that the SPIO particles are mostly uniform in size distribution (see Supporting Information). Compared to previously studied hydrophilic SPIO particles that are synthesized through co-precipitation of ferrous (Fe^{2+}) and ferric (Fe^{3+}) ions in a basic aqueous phase,[8,13] our particles are covered with hydrophobic aliphatic chains from oleic acid and oleylamine during SPIO synthesis, which is essential for micelle encapsulation. SPIO-loaded polymeric micelles were formed using a solvent-evaporation procedure,[7] in which a cluster of SPIO particles was encapsulated inside the hydrophobic core of PCL-*b*-PEG micelles. In addition to SPIO-polymeric micelles, we also formed lipid micelles containing single SPIO particles by using 1,2-diacyl-*sn*-glycero-3-phosphoethanolamine-*N*-[methoxy(polyethylene glycol)-5000] (DSPE-PEG5k) lipid (TEM verified the single SPIO micelles, see Supporting Information). It is noteworthy that peptide-based copolymers have also been used to form polymer micelles or vesicles for encapsulation of both hydrophilic and hydrophobic maghemite nanocrystals.[14,15] Recently, Lecommandoux and co-workers reported the development of deformable maghemite-loaded, polybutadiene-*b*-poly(glutamic acid) vesicles under an external magnetic field, which may provide a responsive nanosystem for controlled drug delivery.[15] In this study, we choose

[*] Prof. J. Gao, Dr. H. Ai, B. Weinberg, Dr. X.-T. Shuai, Prof. M. D. Pagel
Department of Biomedical Engineering
Case Western
Reserve University
Cleveland, OH 44106 (USA)
E-mail: jinming.gao@case.edu
Dr. C. Flask, Prof. J. Duerk
Department of Radiology, Case Western Reserve University
Cleveland, OH 44106 (USA)
Prof. D. Farrell
Department of Physics, Case Western Reserve University
Cleveland, OH 44106 (USA)

[**] This research is supported by the National Institute of Health (NIH RO1-90696). We are also grateful to a DOD postdoctoral fellowship to H. Ai, a DOD predoctoral fellowship to B. Weinberg, and a fellowship support from the Ohio Biomedical Research and Technology Trust fund to X.-T. Shuai. Supporting Information is available online from Wiley InterScience or from the author.

 DOI: 10.1002/adma.200401904

ADVANCED MATERIALS

biocompatible and biodegradable PCL-*b*-PEG copolymer for the formation of SPIO-loaded micelles and specifically examined their applications as ultrasensitive MR probes.

SPIO-loaded polymeric micelles were analyzed by dynamic light scattering (DLS) to determine the size distribution in aqueous solution, inductively coupled plasma–atomic emission spectroscopy to measure iron concentration, and TEM to examine the SPIO distribution in polymeric micelles. Table 1 provides the physico-chemical properties of different micelle formulations. Single 4 nm SPIO micelles formed with DSPE-PEG5k lipid had the smallest hydrodynamic diameter of 17 ± 1 nm, while polymeric PCL-*b*-PEG micelles were larger. The mean hydrodynamic diameter of 16 nm SPIO-loaded PCL-*b*-PEG micelles was 110 ± 9 nm (Fig. 2A), while the mean hydrodynamic diameters were 75 ± 4 and 97 ± 6 nm for PCL-*b*-PEG micelles containing 4 and 8 nm SPIO particles, respectively. The magnetite-nanoparticle loading density (in wt.-%) was 19.5, 38.1, and 54.2 % for 4, 8, and 16 nm SPIO micelles, respectively. An increase in SPIO diameter resulted in an increase in SPIO-loading density as well as in micelle diameter. We also examined micelle samples using TEM and verified the clustering of SPIO nanoparticles in the micelle cores. Figure 2B shows isolated clusters of SPIO nanoparticles on a carbon-coated grid at low magnification. Closer examination of a single micelle particle revealed the clustering of multiple 16 nm SPIO nanoparticles (Fig. 2C). Interestingly, TEM analysis (Fig. 2D) of the same 16 nm SPIO-micelle sample after negative staining by 2 % phosphotungstic acid (PTA) established that clustered SPIO particles were encapsulated inside the "bright" unstained hydrophobic cores of PCL-*b*-PEG micelles. In addition to above SPIO-clustered micelles, single and small aggregates (2–3 units) of SPIO particles were also observed in TEM images (Figs. 2B,D). These aggregate structures represent the variation in SPIO loading inside polymeric micelles, which may reflect the polydisperse nature of the PCL-*b*-PEG copolymer and the resulting micelles. Encapsulation of SPIO nanoparticles inside the hydrophobic micelle cores has the advantages of avoiding potential exposure of hydrophobic SPIO surfaces and adsorption of blood proteins (e.g., opsonin), and may allow a prolonged blood circulation.

Table 1. Micelle size, SPIO loading density, T_1 and T_2 relaxivities (r_1 and r_2, respectively), and MRI sensitivity for different SPIO-loaded micelle formulations.
Note: r_1 and r_2 values are in the unit of Fe mM^{-1} s^{-1}.

Micelle formulation	Micelle size [nm]	SPIO loading [wt.-%]	r_1	r_2	MRI sensitivity [μg mL^{-1}]
4 nm SPIO DSPE-PEG5k	17±1	12.4	1.3	25.1	450
4 nm SPIO PCL5k-b-PEG5k	75±4	19.5	2.9	169	20.5
8 nm SPIO PCL5k-b-PEG5k	97±6	38.1	1.6	318	6.9
16 nm SPIO PCL5k-b-PEG5k	110±9	54.2	2.0	471	5.2

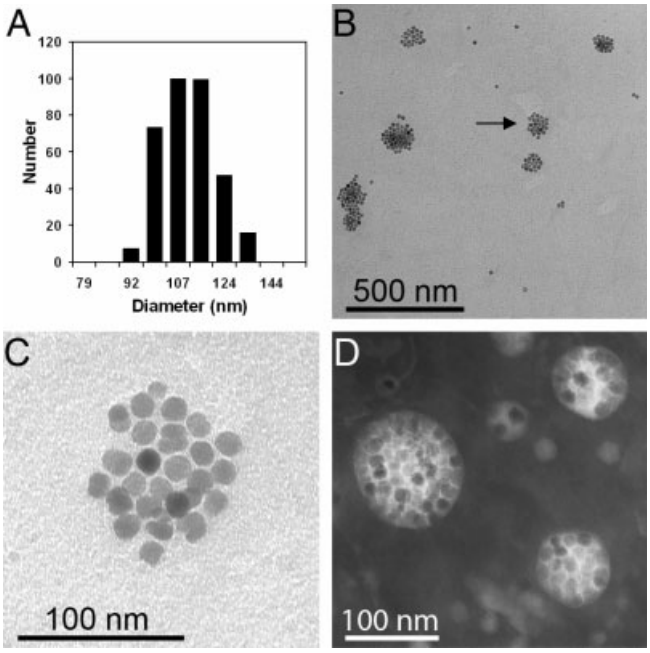

Figure 2. A) DLS histogram showing the size distribution of 16 nm SPIO-loaded polymeric micelles based on PCL5k-*b*-PEG5k copolymer (mean diameter: 110 nm). B) TEM of these micelles at low magnification. Isolated clusters of SPIO particles were observed. C) A high-magnification TEM image of the micelle indicated by the arrow in (B). D) TEM image of the same micelle sample after negative staining by 2 % PTA. SPIO clusters were found to localize inside the "bright" hydrophobic cores of micelles.

T_1 and T_2 relaxivities were measured on a clinical 1.5 T MRI scanner (Table 1). All micelle formulations had comparable r_1 values in the range of 1.3 to 2.9 Fe mM^{-1} s^{-1}, significantly smaller than 20–30 Fe mM^{-1} s^{-1} typical for hydrophilic SPIO in a dextran matrix (e.g., Clariscan, MION-46).[9] The reduced accessibility of water to SPIO particles inside the hydrophobic micelle core may be a major cause for the smaller r_1 values. In contrast, the T_2 relaxivities of SPIO-loaded PCL-*b*-PEG micelles are significantly larger than those for SPIO-dextran particles (30–50 Fe mM^{-1} s^{-1}).[9] The T_2 relaxivity is increased dramatically with SPIO clustering and is further increased by increases in SPIO diameter and loading density. Figure 3A displays the measurement of T_2 relaxivities for two micelle formulations: 4 nm SPIO-loaded-DSPE-PEG5k lipid micelles and 4 nm SPIO-loaded-PCL-*b*-PEG polymeric micelles. The latter has a much larger T_2 relaxivity (r_2 = 169 Fe mM^{-1} s^{-1}) than the former micelles (25.1 Fe mM^{-1} s^{-1}), as is indicated by the steeper slope in Figure 3A. To evaluate the effect of SPIO clustering on MRI images, we compared the MRI signal intensities between these two micelle formulations (Fig. 3B). For a given Fe concentration, multiply loaded micelles showed a significantly darker (T_2-weighted) image than those containing just one particle, confirming that SPIO clustering drastically increases image contrast. Although re-

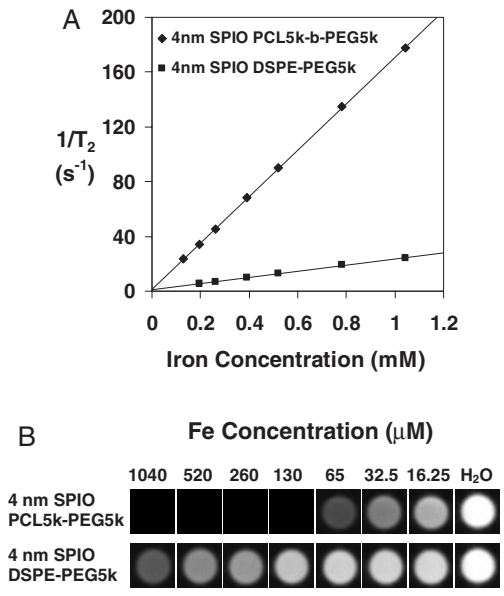

Figure 3. A) T_2 relaxation rates ($1/T_2$, s^{-1}) as a function of iron concentration (mM) for 4 nm SPIO-loaded PCL5k-*b*-PEG5k polymeric micelles and DSPE-PEG5k lipid micelles (1.5 T, 25 °C). B) T_2-weighted MRI images (1.5 T, spin-echo sequence: repetition time TR = 5000 ms, echo time TE = 40 ms) of the above two micelle formulations.

laxation theory for single SPIO particles has been developed,[16] no quantitative microscopic theory is available to explain the T_2 relaxivity changes for clustered SPIO particles. Our preliminary magnetization data confirmed the superparamagnetic character of the embedded particles and showed that their (saturation) magnetic moment per unit mass of Fe at 1.5 T is relatively insensitive to changes in clustering or aggregation. This suggests that the interaction of water molecules with SPIO-micelles plays an important role in the T_2 relaxivity changes. This new experimental platform provides a well-characterized model system that can potentially help elucidate the mechanisms of MRI relaxivity and their dependence on the underlying microscopic parameters.

To quantify the MRI detection limit, we define the sensitivity as the micelle concentration at which the MRI signal intensity decreases to 50 % of that for pure water in T_2-weighted images (1.5 T, spin-echo sequence: TR = 5000 ms, TE = 80 ms). For 4 nm SPIO nanoparticles, the PCL-b-PEG micelle formulation gives a detection limit of 20.5 $\mu g\,mL^{-1}$ compared to 450 $\mu g\,mL^{-1}$ for DSPE-PEG5k formulation (Table 1). Furthermore, for PCL-*b*-PEG micelles loaded with 16 nm SPIO particles, the sensitivity limit drops further to 5.2 $\mu g\,mL^{-1}$. Since the molecular weight of typical micelles is on the order of 10^6 $g\,mol^{-1}$,[3] the above sensitivity limit corresponds to an approximately 5 nM micelle concentration. This sensitivity may prove to be essential in detecting low concentrations of receptors for molecular-imaging applications. To verify this, we are currently conducting experiments to functionalize the surface of SPIO-polymeric micelles with a cyclic Arg-Gly Asp ligand[17] to target the $\alpha_v\beta_3$ integrin receptors inside the tumor vasculature for angiogenesis imaging in vivo.

In conclusion, this paper represents the first proof of concept using superparamagnetic polymeric micelles with ultrasensitive MRI detection on a 1.5 T clinical MRI scanner. Clustering of monodisperse SPIO particles inside the hydrophobic core of micelles results in high SPIO loading and a considerable increase in MRI relaxivity. The hydrophilic PEG corona provides a protective shell for stabilizing particles in aqueous solution. The unique nanocomposite design expands the applications of polymeric micelles, not only for encapsulation of small organic molecules, but also for nanoscopic hydrophobic particles aimed at novel diagnostic and therapeutic applications.

Experimental

Syntheses of Magnetite Nanoparticles: Following reported procedures by Sun et al. [11,12], we first synthesized the 4 nm magnetite (Fe_3O_4) nanoparticles. Briefly, $Fe(acac)_3$ (2 mmol; acac = acetylacetonate) was mixed in phenyl ether (20 mL) with 1,2-hexadecanediol (10 mmol), oleic acid (6 mmol), and oleylamine (6 mmol) under nitrogen. The mixture was then heated to reflux (265 °C) for 30 min. After cooling to room temperature, the solution was treated with ethanol under air to yield a dark-brown precipitate. The product was resuspended in hexane in the presence of oleic acid and oleylamine and reprecipitated with ethanol to give 4 nm Fe_3O_4 nanoparticles. The 6 nm Fe_3O_4 nanoparticles were synthesized by replacing phenyl ether solvent with benzyl ether (20 mL) and heating to reflux (~300 °C) under nitrogen for 1 h. We used 6 nm Fe_3O_4 nanoparticles as seeds to synthesize larger monodisperse magnetite nanoparticles of 8 and 16 nm in diameter following the procedure by Sun et al. [12].

Synthesis of Diblock PCL5k-b-PEG5k Copolymer: A detailed synthetic procedure for PCL-*b*-PEG copolymers was described in a recent publication from our lab [7]. Briefly, ring-opening polymerization of ε-caprolactone using monomethoxy poly(ethylene glycol) (5 kDa) as a macroinitiator and $Sn(Oct)_2$ as a catalyst was carried out at 115 °C for 24 h. After synthesis, the copolymer was dissolved in tetrahydrofuran (THF) and precipitated with the addition of hexane (95 % yield). The resulting copolymer was characterized by gel permeation chromatography (GPC, PLgel 5 μm Mixed-D 300 × 7.5 mm column, Polymer Laboratories) with THF as an eluent (1 mL min^{-1}). The degree of polymerization of the PCL block was calculated by comparing integrals of characteristic peaks of the PCL block at ~2.25 ppm (triplet, –C(=O)–CH_2–) and PEG block at 3.35 ppm (singlet, –OCH_3) in the ^{1}H NMR spectrum (Varian 600 MHz spectrometer). Both GPC and ^{1}H NMR data confirmed the PCL5k-*b*-PEG5k composition and molecular weight.

Relaxivity Measurement: For different SPIO-micelle formulations, T_1 and T_2 relaxivities were measured at 1.5 T on a clinical MRI scanner (Siemens Sonata) at room temperature. A birdcage receive coil (inner diameter = 260 mm) was used to provide high signal-to-noise images and a homogeneous receive field over the field of view of the contrast agent solutions. A standard FLASH (fast low angle shot) gradient-echo sequence was used to acquire the T_1-weighted images. The T_1-weighted images were obtained by using a short echo time (TE ~ 4 ms) while varying the repetition time (TR) of the acquisition (20 ~ 500 ms). The T_2-weighted images were acquired with a conventional spin-echo acquisition (TR = 5000 ms) with TE values ranging from 11 to 90 ms. For the T_1-weighted scans, 5–10 signal averages were required to limit the effects of noise on the relaxivity measurements. Finally, the relaxivity values, r_1 and r_2, were calculated through the least-squares curve fitting of 1/relaxation time (s^{-1}) versus the iron concentration (mM Fe).

Received: November 19, 2004
Final version: May 3, 2005

ADVANCED MATERIALS

[1] V. P. Torchilin, *Adv. Drug Delivery Rev.* **2002**, *54*, 235.
[2] H. Otsuka, Y. Nagasaki, K. Kataoka, *Adv. Drug Delivery Rev.* **2003**, *55*, 403.
[3] M. L. Adams, A. Lavasanifar, G. S. Kwon, *J. Pharm. Sci.* **2003**, *92*, 1343.
[4] B. Dubertret, P. Skourides, D. J. Norris, V. Noireaux, A. H. Brivanlou, A. Libchaber, *Science* **2002**, *298*, 1759.
[5] S. Lecommandoux, Y. Gnanou, *Bioforum* **2004**, *5*, 38.
[6] X. Shuai, T. Merdan, A. K. Schaper, F. Xi, T. Kissel, *Bioconjugate Chem.* **2004**, *15*, 441.
[7] X. Shuai, H. Ai, N. Nasongkla, S. Kim, J. Gao, *J. Controlled Release* **2004**, *98*, 415.
[8] T. Shen, R. Weissleder, M. Papisov, A. Bogdanov, T. J. Brady, *Magn. Reson. Med.* **1993**, *29*, 599.
[9] Y. J. Wang, S. M. Hussain, G. P. Krestin, *Eur. J. Radiol.* **2001**, *11*, 2319.
[10] S. M. Moghimi, A. C. Hunter, J. C. Murray, A. Szewczyk, R. Savic, L. Luo, A. Eisenberg, D. Maysinger, *Science* **2004**, *303*, 626.
[11] S. Sun, H. Zeng, *J. Am. Chem. Soc.* **2002**, *124*, 8204.
[12] S. Sun, H. Zeng, D. B. Robinson, S. Raoux, P. M. Rice, S. X. Wang, G. Li, *J. Am. Chem. Soc.* **2004**, *126*, 273.
[13] K. E. Kellar, D. K. Fujii, W. H. Gunther, K. Briley-Saebo, M. Spiller, S. H. Koenig, *Magn. Reson. Mater. Phys., Biol. Med.* **1999**, *8*, 207.
[14] L. E. Euliss, S. G. Grancharov, S. O'Brien, T. J. Deming, G. D. Stucky, C. B. Murray, G. A. Held, *Nano Lett.* **2003**, *3*, 1489.
[15] S. Lecommandoux, O. Sandre, F. Checot, J. Rodriguez-Hernandez, R. Perzynski, *Adv. Mater.* **2005**, *17*, 712.
[16] S. H. Koenig, K. E. Kellar, *Magn. Reson. Med.* **1995**, *34*, 227.
[17] N. Nasongkla, X. Shuai, H. Ai, B. D. Weinberg, J. Pink, D. A. Boothman, J. Gao, *Angew. Chem. Int. Ed.* **2004**, *43*, 6323.

In-Plane Aligned $Pb(Zr_xTi_{1-x})O_3$ Microbelts Fabricated by Near Migration and Restricted Growth**

By *Wen Gong*, *Jing-Feng Li*,* *Chun-E Peng*, *Zhi Lun Gui*, and *Long Tu Li*

Microelectromechanical systems (MEMS) and nanoelectromechanical systems (NEMS), which take advantage of well-established integrated-circuit manufacturing methods, continue to be an exciting multidisciplinary field with tremendous progress taking place in research and commercialization. The trend toward integration and miniaturization in MEMS and NEMS drives the development of interrelated smart materials such as ferroelectric and piezoelectric materials. Lead zirconate titanate ($Pb[Zr_xTi_{1-x}]O_3$, PZT) with outstanding piezoelectricity provides an excellent candidate as a smart material for use in MEMS and NEMS. Great efforts have therefore been taken to fabricate PZT micro- and nanostructures by downsizing existing PZT films using conventional microfabrication methods.[1] In the past decade since the discovery of carbon nanotubes,[2] the synthesis of one-dimensional (1D) materials has become the focus of intensive research because of their fundamental characteristics and potential applications. 1D micro- and nanomaterials with various microstructures, such as tubes,[3] belts,[4] wires,[5] and rods,[6] have been prepared by different synthetic routes.[7] For instance, a 1D zinc oxide nanostructure was extensively investigated for its dual semiconducting and piezoelectric properties.[4] Some scientists have attempted to fabricate 1D PZT microstructures by using unconventional methods based on physical or chemical synthesis to provide an alternative and intriguing strategy to overcome fundamental limitations of conventional microfabrication. For example, Wang et al. synthesized PZT fibers with diameters ranging from 500 nm to several micrometers using electrospinning and metallo-organic decomposition techniques.[8] By using sol–gel template electrophoresis synthesis methods, Limmer et al. prepared PZT nanorods with diameters of 70–150 nm and lengths of 10 μm.[9] However, in their methods there are some difficulties in assembly of the PZT fibers or rods for the construction of devices.

In this paper, we propose the synthesis of self-assembled PZT microbelts by using a simple method. Long and thin PZT belt-type crystals, 50–150 μm long, 60–300 nm thick, and 1–2 μm wide, were prepared on $SrTiO_3$ (STO) monocrystal wafers with gold microparticles on the surface of the wafers. Details of the preparation procedure are given in the Experimental section.

Figure 1 shows optical microscopy images of the PZT microbelts on STO(100) wafers, which were annealed at 930–970 °C for 60 min in air. Well-aligned PZT microbelts with a width of 1–2 μm and a length of over 50 μm were grown on STO(100) substrates. The maximum length of the PZT microbelts reached 150 μm. Because of the limitations of optical microscopy, the microstructures of much finer PZT microbelts are not shown here. Figure 1A shows PZT microbelts annealed at a lower temperature (930 °C). All the PZT microbelts developed along the $<110>_{STO}$ direction, being parallel with or perpendicular to each other. However, increasing the annealing temperature could interfere with the well-aligned growth of PZT microbelts (Fig. 1B). After annealing at 970 °C, the microbelts formed an interlacing pattern with certain alternate angles, for instance, 90°, 45°, and 26°, indicating that the PZT microbelts developed not only along the $<110>_{STO}$ direction but also along the $<100>_{STO}$ or other high-index directions. It was noted that every PZT microbelt is enclosed by several gold particles. Figure 1C shows the atomic force microscopy (AFM) image of a PZT microbelt selected from the same sample presented in Figure 1A. By using a silicon tip in contact mode, all the gold particles were removed. As shown in the AFM image and the line profile, it

[*] Prof. J.-F. Li, Dr. W. Gong, C.-E Peng, Prof. Z. L. Gui, Prof. L. T. Li
State Key Laboratory of New Ceramics and Fine Processing
Department of Materials Science and Engineering
Tsinghua University
Beijing, 100084 (P.R. China)
E-mail: jingfeng@mail.tsinghua.edu.cn

[**] This work was supported by the Ministry of Science and Technology (2002CB613306) and the National Natural Science Foundation of China (50325207).

  DOI: 10.1002/adma.200500340